The Emerald Research Register for this journal is available at
www.emeraldinsight.com/researchregister

The current issue and full text archive of this journal is available at
www.emeraldinsight.com/0961-5539.htm

Numerical analysis of vortex shedding behind a porous square cylinder

Tswen-Chyuan Jue

Department of Vehicle Engineering, National Huwei Institute of Technology, Yunlin, Taiwan, Republic of China

Received September 2002
Revised June 2003
Accepted September 2003

Keywords *Porous materials, Numerical analysis*

Abstract *Vortex shedding behind a porous square cylinder is studied by a semi-implicit projection finite element method in this paper. Flow fields over the porous square cylinder with various porosity and Darcy number were calculated to investigate the effects of porous media on Strouhal number, lift and drag coefficients at Re = 100, 200 and 250. The global quantities of the shedding flow appear evident variation for Da varied from 10^{-5} to 10^{-4}. In particular, Strouhal number displays an obvious jump for Da = 10^{-4} at Re = 250, due to the variation in flow structure near the cylinder. Larger Darcy number postpones the occurrence of flow fluctuation, and the oscillation flow presents stronger amplitude. However, the flow field and the characteristic values of vortex shedding for Da ≤ 10^{-6} are almost not changed. For different porosity, time histories of C_D and C_L look similar. In conclusion, Darcy number demonstrates more influence on the flow field than porosity does.*

Nomenclature

C_D = drag coefficient $D/(\rho U_\infty^2/2)$
C_L = lift coefficient $L/(\rho U_\infty^2/2)$
D = drag force
Da = Darcy number K/H^2
f = vortex shedding frequency
g = acceleration of gravity
H = height of cylinder
K = permeability
L = lift force
$\mathbf{n}$ = normal vector
p = pressure
P = dimensionless pressure $p/\rho U_\infty^2$
Re = Reynolds number $U_\infty H/\nu$
St = Strouhal number fH/U_∞
t = time
$\mathbf{u}$ = velocity vector
$\mathbf{U}$ = dimensionless velocity vector $\mathbf{u}/U_\infty$
U_∞ = free stream velocity
U = x direction dimensionless velocity
V = y direction dimensionless velocity
$\mathbf{X}$ = dimensionless Cartesian coordinate vector
x, y = Cartesian coordinate

Greek symbols

Γ = boundary
σ = stress
ε = porosity
ν = kinematic viscosity
ρ = density of fluid
τ = dimensionless time tU_∞/H

Superscripts

$n, n+1$ = nth, $n+1$th time step

Subscripts

0 = initial value
p = shedding period

The author gratefully acknowledges the financial support of this study by the National Science Council of the Republic of China, under contract NSC89-2212-E-150-044.

International Journal of Numerical Methods for Heat & Fluid Flow
Vol. 14 No. 5, 2004
pp. 649-663

0961-5539
DOI 10.1108/09615530410539964

Introduction

Vortex shedding behind bluff bodies such as circular cylinders, rectangular cylinders has been studied in detail to understand the appearance and structure of flow vortexes due to its practical applications in the design of road vehicles, tower buildings, heat exchangers, etc. Many factors can affect the characteristics of vortex shedding including the Reynolds number, the flow conditions, the shape and conditions of bodies. Abundant research had been done (Davis and Moore, 1982; Knisley, 1990; Okajima, 1982; Sarpkaya, 1999) to provide the numerical or experimental data about lift coefficient, drag coefficient, base pressure and Strouhal frequency in this flow. Most of the studies focused on flow past impermeable bodies, but the flow behind a porous body has not been broadly investigated. However, some real conditions such as the heat transfer enhancement of porous inserts in flow field (Martin *et al.*, 1998), the instability of segmented solid propellant rocket motors (Couton *et al.*, 1997), and the use of porous plates as motion damping devices (Downie *et al.*, 2000) are deeply affected by the existence of a porous body. Therefore, an in-depth investigation in the flow past a porous obstruction will be necessary to accumulate more information for relating applications.

For most research about flow behind porous blocks, they concentrated on the steady-state convection heat transfer phenomena (Chikh *et al.*, 1998; Huang and Vafai, 1993; Martin *et al.*, 1998). About vortex flow, Cohen (1991) theoretically investigated the flow over a circular cylinder with surface suction and blowing, and derived a model for St-Re relationship by order of magnitude estimating. Ling *et al.* (1993) numerically verified this model for flow over a square cylinder and reached a similar trend between Strouhal and Reynolds numbers. In these studies, the effects of porous blocks were induced by assigning a velocity boundary condition on the square cylinder. The real phenomena for fluid flowing through a porous block were not simulated in their research.

The purpose of this study is to realize the features of fluid flows behind a square porous cylinder. A general non-Darcy porous media model is adopted to describe the flows both inside and outside the cylinder. Effects of permeability, porosity and Reynolds number on lift and drag coefficients and Strouhal frequency are studied. Steady-state characteristic values and time history of global quantities with vortex shedding are involved in the results.

Mathematical model

A two-dimensional, laminar, and incompressible flow past a porous square cylinder is considered here (Figure 1(a)). The fluid is Newtonian and the properties of the fluid are assumed to be constant. The porous cylinder is considered to be homogeneous, isotropic and saturated with a single-phase fluid. To account for viscous and inertia effects in the porous region, a generalized porous medium flow model (Nithiarasu *et al.*, 1997) is used.

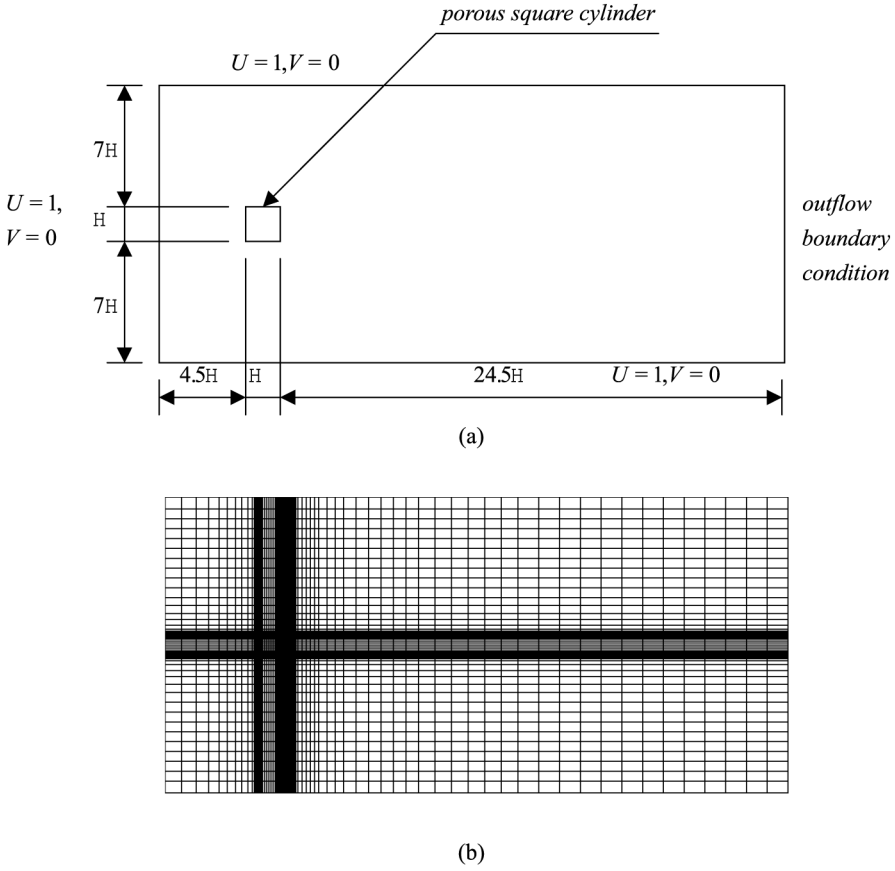

Figure 1.
Flow past a porous square cylinder: (a) problem definition; and (b) finite element mesh

The fluid motion is then governed by the following non-dimensionalized equations:

Continuity equation:

$$\nabla \cdot \mathbf{U} = 0 \tag{1}$$

Momentum equation:

$$\frac{1}{\varepsilon}\frac{\partial \mathbf{U}}{\partial \tau} + \frac{1}{\varepsilon^2}\mathbf{U}\nabla \cdot \mathbf{U} = -\nabla P + \frac{1}{\varepsilon \mathrm{Re}}\nabla^2 \mathbf{U} - \frac{1}{\mathrm{DaRe}}\mathbf{U} - \frac{1.75}{\sqrt{150}}\frac{1}{\sqrt{\mathrm{Da}}}\frac{|\mathbf{U}|}{\varepsilon^{3/2}}\mathbf{U} \tag{2}$$

As described by Chikh *et al.* (1998), the momentum equation in fluid region can be obtained by assigning the porosity ε and Darcy number Da to be unity and a very large number in equation (2), respectively. In this research, a value 10^7 is assigned for Darcy number in the fluid region as that used in the research of

Nithiarasu *et al.* (1997). Referring to Chikh *et al.* (1998), a harmonic mean is adopted to treat the sudden change between clear fluid and porous medium, as suggested by Patankar (1980). In this research, physical variables (**U**, P) are solved by a finite element method, and the construction of stiffness matrix for the points on the interface accumulates the influence from porous and clear areas. This procedure is similar to adopting a harmonic mean for the interfacial values. In addition, the finest mesh is placed on the interface to reduce the sudden change in flow medium (Figure 1(b)).

To complete the formulation, a set of boundary and initial conditions are required. The Dirichlet boundary condition for velocity may be expressed as:

$$\mathbf{U} = \hat{\mathbf{U}} \quad \text{on} \quad \Gamma_1 \tag{3}$$

where $\hat{\mathbf{U}}$ denotes the function that is given on the boundary Γ_1.

The specified stress boundary condition can be expressed as:

$$\boldsymbol{\sigma} \cdot \mathbf{n} = \hat{\boldsymbol{\sigma}} \quad \text{on} \quad \Gamma_2 \tag{4}$$

where $\hat{\boldsymbol{\sigma}}$ is a specified stress function on the boundary Γ_2. $\Gamma = \Gamma_1 \cup \Gamma_2$, is the boundary of the domain.

The outflow boundary Γ_3 is a part of the boundary Γ_2, however, the pressure itself and the velocity are unknown on Γ_3. An approach used by Shimura and Kawahara (1988) was adopted in this research. The pressure on outflow boundary condition is calculated by taking the normal and tangential derivatives of the Navier-Stokes equations and using the continuity equation. The pressure Poisson equation for the boundary can be obtained as:

$$\left(\frac{\partial^2}{\partial \eta^2} + \frac{\partial^2}{\partial \tau^2}\right) P^{n+1} = 2\frac{\partial \mathbf{U}_\eta^n}{\partial \eta}\frac{\partial \mathbf{U}_\tau^n}{\partial \tau} - 2\frac{\partial \mathbf{U}_\eta^n}{\partial \tau}\frac{\partial \mathbf{U}_\tau^n}{\partial \eta} \tag{5}$$

An additional Dirichlet boundary condition is required to solve equation (5). The adjacent nodes to the outflow boundary are considered in an approximate sense. The integration of equation (5) for last strip of elements as shown in Figure 2 can be performed and it leads to the following set of equations:

$$[A] \quad \begin{bmatrix} P^{n+1} \\ P^n \end{bmatrix} = \begin{bmatrix} q^n \\ 0 \end{bmatrix} \tag{6}$$

where P^{n+1} on Γ_3 are unknown and P^n on the adjacent nodes are known, A means the Laplacian matrix, and q^n are the velocity gradient vectors on the right hand side of equation (6). In this approach, only the pressure at time $t = 0$ is necessary to solve the boundary pressure Poisson equation (6).

Let the initial condition be given by:

$$\mathbf{U}(\mathbf{X}, 0) = \mathbf{U}_0(\mathbf{X}) \tag{7}$$

Then it is required to satisfy the incompressibility condition,

$$\nabla \cdot \mathbf{U}_0 = \mathbf{0} \tag{8}$$

and

$$\mathbf{n} \cdot \mathbf{U}_0 = \mathbf{n} \cdot \hat{\mathbf{U}} \tag{9}$$

Method of solution

A projection scheme (Chorin, 1968, Nithiarasu *et al.*, 1996) is used for the temporal discretization. The Adams-Bashforth scheme is adopted to treat the advanced terms and an implicit Euler scheme is applied for the diffusion terms. The solution procedure is as follows.

Step 1: A set of equations is solved without inclusion of the pressure term.

$$\frac{1}{\varepsilon}\left(\frac{\tilde{\mathbf{U}}^{n+1} - \mathbf{U}^n}{\Delta\tau}\right) = -\frac{1}{\varepsilon^2}\left[\frac{3}{2}(\mathbf{U}\cdot\nabla\mathbf{U})^n - \frac{1}{2}(\mathbf{U}\cdot\nabla\mathbf{U})^{n-1}\right] + \frac{1}{\varepsilon \mathrm{Re}}\nabla^2\mathbf{U}^{n+1} - \frac{1}{\mathrm{Da}\,\mathrm{Re}}\mathbf{U}^{n+1} - \frac{1.75}{\sqrt{150}}\frac{1}{\sqrt{\mathrm{Da}}}\frac{|\mathbf{U}|}{\varepsilon^{3/2}}\mathbf{U} \tag{10}$$

where $\tilde{\mathbf{U}}^{n+1}$ is a provisional value for velocity.

Step 2. The pressure is obtained from a Poisson equation including $\tilde{\mathbf{U}}^{n+1}$.

$$\nabla^2 P^{n+1} = \frac{1}{\varepsilon\Delta\tau}\nabla\cdot\tilde{\mathbf{U}}^{n+1} \tag{11}$$

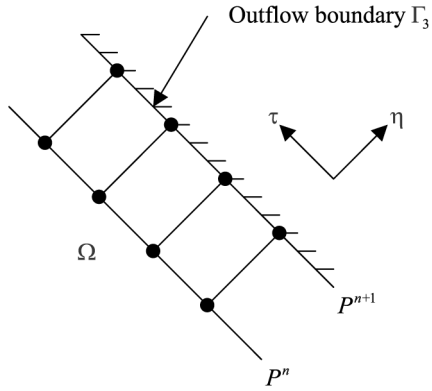

Figure 2.
Outflow boundary condition

Step 3. The real velocity is calculated by correcting the provisional velocity with the pressure effect.

$$\mathbf{U}^{n+1} = \tilde{\mathbf{U}}^{n+1} - \varepsilon \Delta \tau \nabla P^{n+1} \tag{12}$$

A Galerkin finite element method is used for the above equations in spatial discretization to yield several sets of simultaneous linear equations solved by a direct method. In order to reduce the sudden variation on the interface between the fluid and porous region, the finest mesh (0.05×0.05) is used next to the interface and enlarged gradually. A grid independence study was carried out with several different meshes. The values of shedding period, drag coefficient and lift coefficient for different meshes are listed in Table I. Because of the computational cost and accuracy considerations, the 55×79 non-uniformed mesh (Figure 1(b)) was used in this study. In addition, the code was validated by comparing the results with those of Davis and Moore (1982) for flow past a non-porous cylinder (Table II). The agreement between the present result and their results is satisfactory.

Results and discussion

The main purpose of this research is to numerically determine the effects of porous properties on the characteristics of vortex shedding. According to Chung and Kang's (2000) description, it is difficult to experimentally or numerically observe the vortex structure at a high Reynolds number. In addition, Sohankar *et al.* (1999) presented results that the transition from 2D to 3D shedding flow occurred at Re= 160-200. In considering the flow past a porous cylinder, the above range of Reynolds number will shift to larger values due to less obstruction for fluid flow. Therefore, Reynolds number 100, 200 and 250 were chosen in this study. On the other hand, porosity ε relating to

Table I.
Grid independent test at $\mathrm{Re} = 100$, $\varepsilon = 0.4$, and $\mathrm{Da} = 10^{-4}$

Mesh	Shedding period	C_L	C_D
53×71	6.46	−0.307-0.307	1.604-1.656
55×79	6.47	−0.314-0.314	1.604-1.656
61×85	6.47	−0.318-0.318	1.603-1.656

Table II.
Comparison of global quantities with literature

Source	Re	St	C_{Dav}
Davis and Moore[a]	100	0.148-0.153	1.64
	200	0.158-0.165	1.71
Present method	100	0.154	1.60
	200	0.160	1.72

Note: [a]Numerical results with several meshes

the ratio of void volume to total volume is set to be 0.4-0.8. Because it is very difficult to obtain a Darcy number up to 10^{-2} experimentally (Lage, 1992), Darcy number, Da, is assigned as 10^{-4}-10^{-8} in the present analysis.

First, the flows of Re = 200 were studied. The plot domain is confined in $x = 3.8$-15.4 and $y = 5.5$-9.5 to clearly scrutinize flow vortex. Figure 3 shows the streamlines of $\varepsilon = 0.4$ and $\mathrm{Da} = 10^{-4}$ for lift coefficient at maximum, zero and minimum conditions. At $C_{L\max}$, a circulation appears behind the upper area of the cylinder. Later the circulation moves forward and develops larger at $C_L = 0$. The vortex continuously moves downstream and combines with the main flow. Meanwhile, a small vortex has been developing in the lower area behind the cylinder at C_{Lmin} condition. To study the effects of porous media, a different Darcy number 10^{-8} is chosen for the next case and the porosity is kept the same. In Figure 4, the main pattern is similar to Figure 3, but the positions and sizes of circulations are different. There is a phase angle difference between these two conditions. Obviously, a smaller Darcy number implies the cylinder with a smaller permeability and results in various vortex strength and phase angle. In Figure 5(a), the streamlines at $C_{L\max}$ are shown for $\varepsilon = 0.8$,

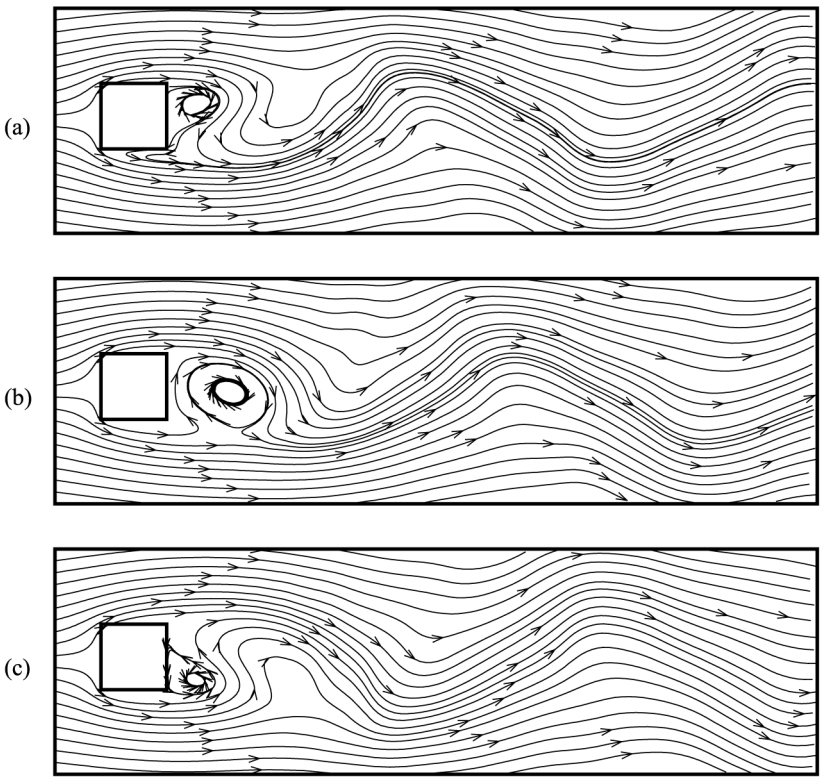

Figure 3.
Streamline contours at Re = 200, $\varepsilon = 0.4$, $\mathrm{Da} = 10^{-4}$: (a) C_L=max; (b) C_L=0; and (c) C_L=min

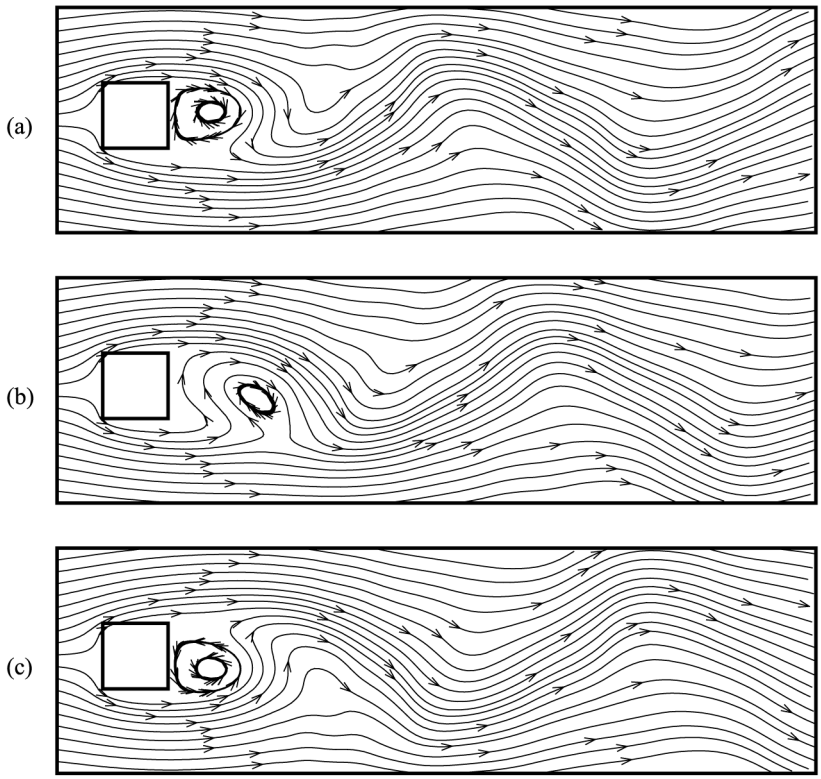

Figure 4.
Streamline contours at $Re = 200$, $\varepsilon = 0.4$, $Da = 10^{-8}$: (a) C_L=max; (b) C_L=0; and (c) C_L=min

$Da = 10^{-4}$ and $Re = 200$. A larger porosity corresponds to more void volume in the cylinder for fluid to flow through and this effect induces a different vortex size and phase angle in the vortex street. About the influence of Reynolds number, Figure 5(b) and (c) demonstrate the flow field at $Re = 250$. Comparing with Figure 3(a), the stronger vortex stream penetrates the cylinder at $Da = 10^{-4}$ causing the variations in the size and position of the vortex (Figure 5(b)). Nevertheless, the vortex flow for $Da = 10^{-8}$ cannot penetrate the cylinder due to the cylinder with smaller permeability. For further understanding the detail of fluid flow in the porous cylinder, the streamlines and velocity vectors inside and outside the porous cylinder are shown in Figure 6 for those cases shown in Figure 5. The flow can easily penetrate the porous region in a larger Darcy number as shown in Figure 6(a) and (b). However, the porous cylinder seriously obstructs the fluid flow as Darcy number is reduced to 10^{-8} (Figure 6(c)).

In addition to the streamline structure, a study of flow evolution and characteristic values for different Darcy number and porosity is interesting to researchers. In order to track the flow evolution, the drag coefficient and

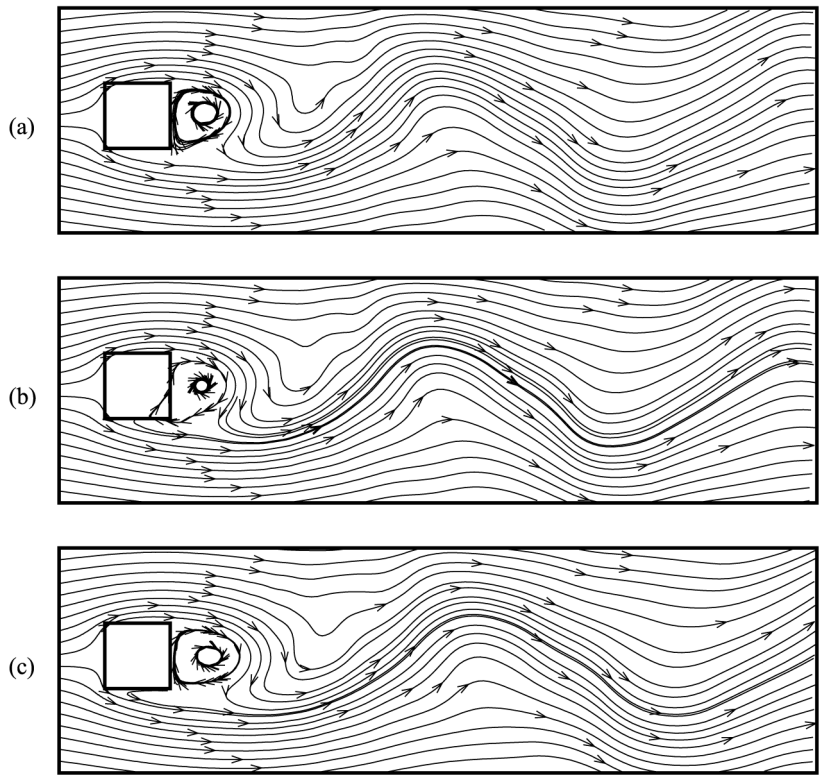

Figure 5.
Streamline contours at C_L=max: (a) Re = 200, $\varepsilon = 0.8$, Da = 10^{-4}; (b) Re = 250, $\varepsilon = 0.4$, Da = 10^{-4}; and (c) Re = 250, $\varepsilon = 0.4$, Da = 10^{-8}

lift coefficient were calculated at each time step and shown in Figures 7 and 8. The C_L and C_D time histories for different Darcy number are shown in Figure 7(a) and (b), respectively. For easily observing the variation after the start of vortex flow, the histories for $\tau < 150$ are not shown. Comparing C_L and C_D curves, the pattern of lift coefficient displays a single-peak oscillation whereas drag coefficient presents a twin-peak pattern. The appearance of vortex shedding for $\mathrm{Da} = 10^{-4}$ is later than those at $\mathrm{Da} = 10^{-6}$ and 10^{-8} because of a larger permeability cylinder allowing fluid to pass more easily, with less disturbance. In addition, the flow of $\mathrm{Da} = 10^{-4}$ presents larger fluctuating amplitude in C_L curve and a bigger shift in C_D curve. For $\mathrm{Da} = 10^{-6}$ flow, the phase angles of C_L and C_D also present a delay from those of $\mathrm{Da} = 10^{-8}$, but the difference is very small. Relating to the numerical results of flow behind a non-porous cylinder at $\mathrm{Re} = 200$, the start of flow fluctuation at about $\tau = 20$ is much earlier than that for a porous cylinder. On the other hand, the effect of porosity is shown in Figure 8 for $\varepsilon = 0.4$, 0.6 and 0.8. Even the phase angle of $\varepsilon = 0.4$ is deferred, but the start of vortex shedding and phase angle for the three

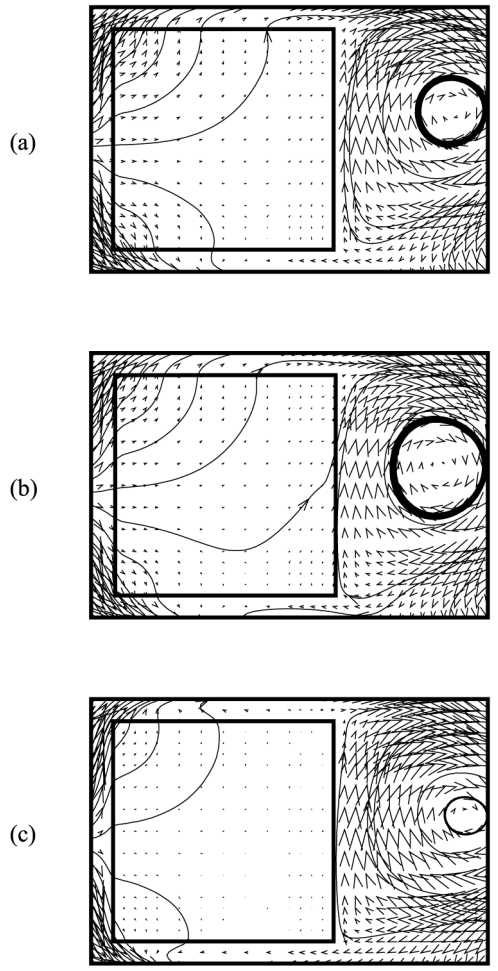

Figure 6.
Streamline contours and velocity vectors near the porous region at C_L=max: (a) Re = 200, $\varepsilon = 0.8$, Da = 10^{-4}; (b) Re = 250, $\varepsilon = 0.4$, Da = 10^{-4}; and (c) Re = 250, $\varepsilon = 0.4$, Da = 10^{-8}

conditions are close. The difference among the three curves in C_D and C_L is small; moreover, the lines for $\varepsilon = 0.6$ and 0.8 are nearly overlapped.

Furthermore, the values of τ_p, C_L and C_D are listed in Table III. In examining the influence of Darcy number, the period of vortex shedding decreases with the increase in Darcy number at $\varepsilon = 0.4$, but the amplitude of lift coefficient enlarges with larger Da only for Re = 100 and 200. This result is caused by the variation in flow field near the cylinder as portrayed in Figures 3(a) and 6(b) and (c). A lower Re flow or a smaller Da cylinder restricts the fluid to flow into the porous cylinder, and varies the relating characteristic values. Similarly, the fluctuating amplitude of drag coefficient enlarges for bigger Da, but the change is not as significant as that in lift coefficient. In contrary to the close values in the range $10^{-8} \leq \text{Da} \leq 10^{-6}$, an obvious jump in the physical quantities is

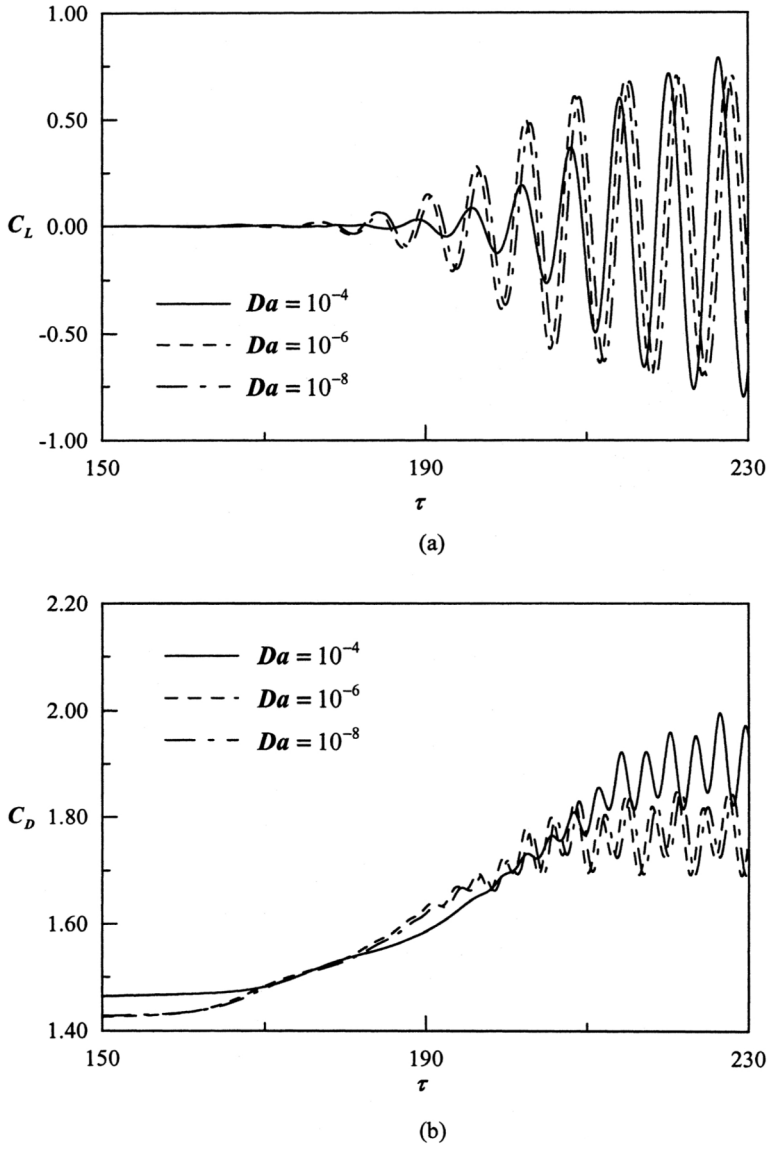

Figure 7.
Time histories at $\mathrm{Re} = 200$, $\varepsilon = 0.4$: (a) lift coefficient; and (b) drag coefficient

found at $\mathrm{Da} = 10^{-4}$ corresponding to larger changes in vortex structure, especially at $\mathrm{Re} = 250$ status. About the influence of porosity, the calculations are conducted for Darcy number 10^{-4} and $0.4 \leq \varepsilon \leq 0.8$. The differences in vortex shedding period, lift and drag coefficients are not as significant as those for different Darcy number. For $\mathrm{Re} = 200$ and 250, τ_p and lift coefficient are reduced with larger porosity, but those at $\mathrm{Re} = 100$ do not follow this trend.

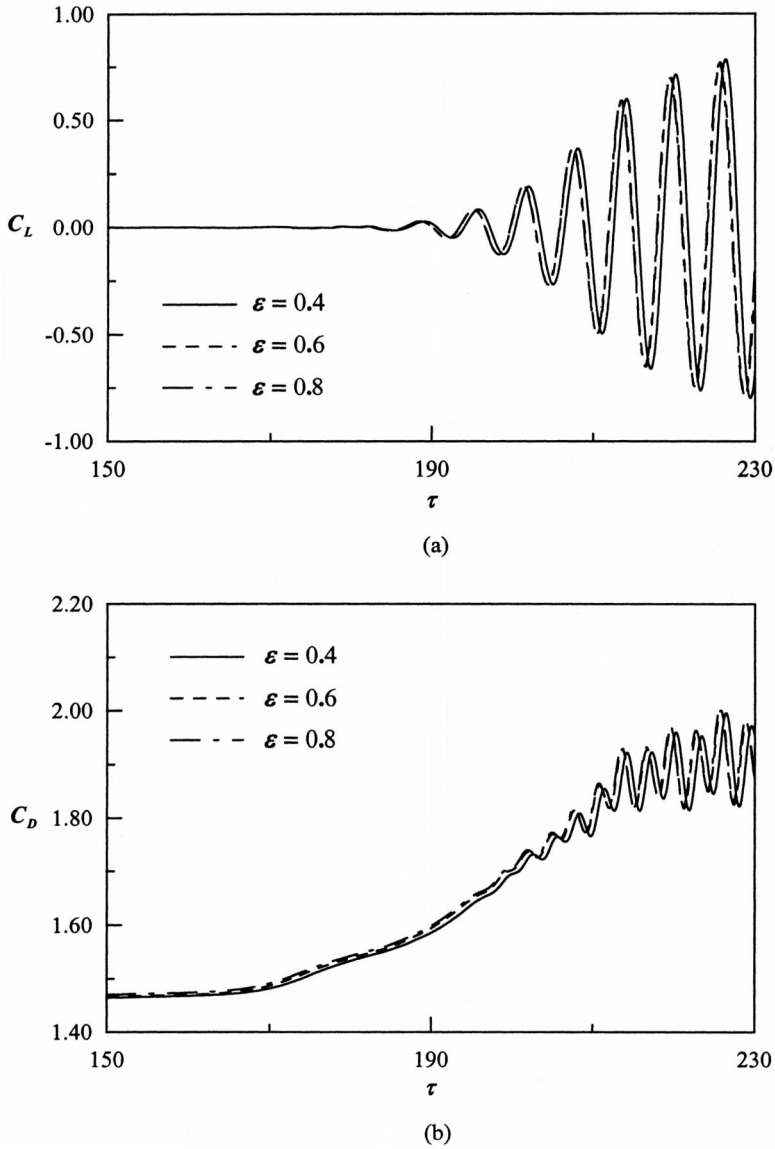

Figure 8.
Time histories at $Re = 200$, $Da = 10^{-4}$: (a) lift coefficient; and (b) drag coefficient

Figure 9 shows the St-Da and St-ε distribution in different Reynolds number. In Figure 9(a), the St values for $Da \leq 10^{-6}$ keep the same and follow the sequence $St_{Re=250} < St_{Re=100} < St_{Re=200}$. This is in contrast to the trend for flow over a non-porous cylinder (Davis and Moore, 1982). However, the Strouhal number becomes gradually larger for $Da > 10^{-6}$. In particular, the $St_{Re=250}$ at

Re	ε	Da	τ_p	C_L	C_D
100	0.4	10^{-8}	6.52	−0.288-0.288	1.559-1.610
	0.4	10^{-7}	6.52	−0.288-0.288	1.559-1.610
	0.4	10^{-6}	6.52	−0.288-0.288	1.559-1.609
	0.4	10^{-5}	6.50	−0.289-0.289	1.557-1.607
	0.4	10^{-4}	6.47	−0.314-0.314	1.604-1.656
	0.5	10^{-4}	6.46	−0.317-0.317	1.609-1.663
	0.6	10^{-4}	6.47	−0.318-0.318	1.614-1.669
	0.7	10^{-4}	6.48	−0.319-0.319	1.619-1.674
	0.8	10^{-4}	6.48	−0.321-0.321	1.623-1.678
200	0.4	10^{-8}	6.37	−0.712-0.712	1.693-1.850
	0.4	10^{-7}	6.37	−0.712-0.712	1.693-1.850
	0.4	10^{-6}	6.37	−0.712-0.712	1.692-1.849
	0.4	10^{-5}	6.35	−0.727-0.727	1.698-1.858
	0.4	10^{-4}	6.22	−0.825-0.825	1.826-2.018
	0.5	10^{-4}	6.20	−0.816-0.816	1.828-2.021
	0.6	10^{-4}	6.19	−0.810-0.810	1.830-2.024
	0.7	10^{-4}	6.18	−0.805-0.805	1.832-2.027
	0.8	10^{-4}	6.17	−0.802-0.802	1.834-2.030
250	0.4	10^{-8}	6.72	−1.077-1.078	1.755-2.017
	0.4	10^{-7}	6.71	−1.077-1.078	1.755-2.017
	0.4	10^{-6}	6.70	−1.074-1.075	1.754-2.016
	0.4	10^{-5}	6.59	−1.072-1.071	1.767-2.034
	0.4	10^{-4}	6.13	−1.024-1.024	1.920-2.189
	0.5	10^{-4}	6.10	−1.007-1.007	1.920-2.189
	0.6	10^{-4}	6.08	−0.988-0.988	1.922-2.191
	0.7	10^{-4}	6.08	−0.988-0.988	1.922-2.191
	0.8	10^{-4}	6.07	−0.983-0.983	1.923-2.193

Table III.
Global quantities with vortex shedding

$\mathrm{Da} = 10^{-4}$ increased to be larger than the other two values. The irregular variation corresponds to a change in vortex structure at this status as described in preceding paragraph. Referring to the effect of porosity, those for $\mathrm{Re} = 250$ and 200 demonstrate a rising trend from $\varepsilon = 0.4$ to 0.8, but the change in different porosity is so small. For $\mathrm{Re} = 100$, the St value remains the same for different porosity.

Conclusion

An analysis of two-dimensional flow over a porous square cylinder has been carried out numerically in this work using a semi-implicit projection finite element method. The generalized porous medium flow model is used to describe the flow in the porous region including inertia, drag and boundary effects. The results show that for flow past a lower permeability cylinder, the vortex occurs earlier and the shedding period is longer. However, the variations of fluctuating amplitude in C_L and C_D mainly depend on Reynolds number causing different flow structures. Moreover, a larger porosity cylinder results

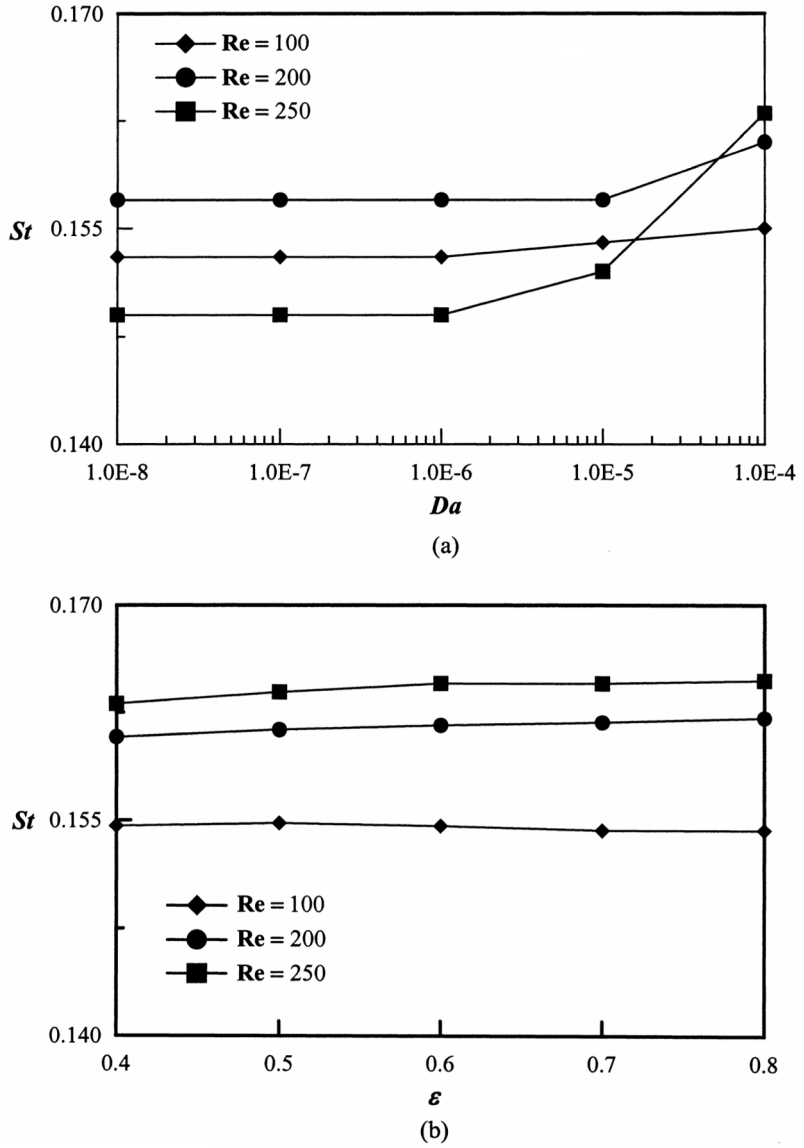

Figure 9.
Strouhal number distribution: (a) St-Da at $\varepsilon = 0.4$; and (b) St-ε at $\mathrm{Da} = 10^{-4}$

in a smaller shedding period, except $\mathrm{Re} = 100$, but the difference is not significant. A deferred phase angle appears in C_D and C_L time histories for smaller porosity cylinders. In particular, there is an obvious jump in physical quantities at $\mathrm{Da} = 10^4$ for $\mathrm{Re} = 250$ resulting in a change in the flow field around the square cylinder.

References

Chikh, S., Boumedien, K., Bouhadef, G. and Lauriat, G. (1998), "Analysis of fluid and heat transfer in a channel with intermittent heated porous blocks", *Heat and Mass Transfer*, Vol. 33, pp. 405-13.

Chorin, A.J. (1968), "Numerical solution of the Navier-Stokes equations", *Mathematics of Computation*, Vol. 22, pp. 745-62.

Chung, Y.J. and Kang, S.H. (2000), "Laminar vortex shedding from a trapezoidal cylinder with different height ratios", *Physics of Fluids*, Vol. 12, pp. 1251-5.

Cohen, R.D. (1991), "Predicting the effects of surface suction and blowing on the Strouhal frequencies in vortex shedding", *JSME International Journal (Series II)*, Vol. 34, pp. 30-9.

Couton, D., Doan-Kim, S. and Vuillot, F. (1997), "Numerical simulation of vortex-shedding phenomenon in a channel with flow induced through porous wall", *International Journal of Heat and Fluid Flow*, Vol. 18, pp. 283-96.

Davis, R.M. and Moore, E.F. (1982), "A numerical study of vortex shedding from rectangles", *Journal of Fluid Mechanics*, Vol. 116, pp. 475-506.

Downie, M.J., Wang, J. and Graham, J.M.R. (2000), "Effectiveness of porous damping devices", *Proceedings of International Offshore and Polar Engineering Conference*, Vol. 3, pp. 418-25.

Huang, P.C. and Vafai, K. (1993), "Flow and heat transfer control over an external surface using a porous block array arrangement", *International Journal of Heat and Mass Transfer*, Vol. 36, pp. 4019-32.

Knisley, C.W. (1990), "Strouhal number of rectangular cylinder at incidence: a review and new data", *Journal of Fluid and Structure*, Vol. 4, pp. 371-93.

Lage, J.L. (1992), "Effect of the convective inertia term on Bénard convection in a porous medium", *Numerical of Heat Transfer, Part A*, Vol. 22, pp. 469-85.

Ling, L.M., Ramaswamy, B., Cohen, D.R. and Jue, T.C. (1993), "Numerical analysis on Strouhal frequencies in vortex shedding over square cylinders with surface suction and blowing", *International Journal of Numerical Methods for Heat & Fluid Flow*, Vol. 3, pp. 357-75.

Martin, A.R., Saltiel, C. and Shyy, W. (1998), "Heat transfer enhancement with porous inserts in recirculating flows", *Journal of Heat Transfer*, Vol. 120, pp. 458-67.

Nithiarasu, P., Seetharamu, K.N. and Sundararajan, T. (1996), "Double-diffusive natural convective heat transfer in a fluid saturated porous medium – a non-Darcy approach", *Numerical Heat Transfer Part A*, Vol. 30, pp. 413-26.

Nithiarasu, P., Seetharamu, K.N. and Sundararajan, T. (1997), "Natural convective heat transfer in a fluid saturated variable porosity medium", *International Journal of Heat and Mass Transfer*, Vol. 40, pp. 3955-67.

Okajima, A. (1982), "Strouhal numbers of rectangular cylinders", *Journal of Fluid Mechanics*, Vol. 123, pp. 255-63.

Patankar, S.V. (1980), *Numerical heat transfer and fluid flow*, Hemisphere Publication Corporation, New York, NY.

Sarpkaya, T. (1999), "Vortex-induced oscillations-a selective review", *Journal of Applied Mechanics*, Vol. 46, pp. 241-58.

Shimura, M. and Kawahara, M. (1988), "Two dimensional finite element flow analysis using the velocity correction method", *JSCE Structure Engineering/Earthquake Engineering*, Vol. 5, pp. 255-63.

Sohankar, A., Norberg, C. and Davidson, L. (1999), "Simulation of three dimensional flow around a square cylinder at moderate Reynolds numbers", *Physics of Fluids*, Vol. 11, pp. 288-306.